Geochemical Perspectives Letters

Decoupling of dissolved and bedrock neodymium isotopes during sedimentary cycling

R.S. Hindshaw[1*], S.M. Aciego[2], A.M. Piotrowski[1], E.T. Tipper[1]

OPEN ACCESS

doi: 10.7185/geochemlet.1828

Abstract

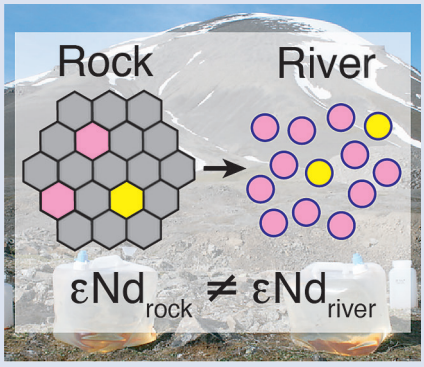

The radiogenic neodymium isotope ratio $^{143}Nd/^{144}Nd$ (expressed as εNd) has been applied to examine seawater elemental budgets, sedimentary provenance, oceanic water mass source and circulation, large scale geochemical cycling, and continental crust growth rates. These applications are underpinned by the assumption that during sedimentary processing the parent/daughter (samarium/neodymium) ratio is conservative during low temperature fluid related processes. In this study, we report εNd data from two streams draining sedimentary formations in the Arctic archipelago of Svalbard. The εNd value of the dissolved load is offset from stream suspended sediment samples by up to 5.5 epsilon units. We demonstrate that dissolved load εNd values are controlled by the dissolution of labile phases present in the catchment rocks which are isotopically distinct from the silicate residue and account for up to 12 % Nd in the bulk sediment. This study highlights; 1) the potential for incongruent release of Nd isotopes to seawater from rocks and sediments, with implications for the isotopic composition of seawater, and 2) the large scale decoupling between a rapidly exchanging labile reservoir and a silicate-bound reservoir during sediment recycling.

Received 20 April 2018 | Accepted 14 October 2018 | Published 8 November 2018

Introduction

Radiogenic neodymium isotopes ($^{143}Nd/^{144}Nd$), commonly reported as εNd (Goldstein and Jacobsen, 1987), have influenced our understanding of geophysical processes, from planetary differentiation to ocean circulation. Continental growth curves are based on εNd values (Taylor and McLennan, 1985) and changes in ocean dynamics and silicate weathering have been inferred from εNd measurements (Piepgras and Wasserburg, 1980; Bayon *et al.*, 2009).

On a finer spatial and temporal scale, variations in the εNd values of seawater recovered from archives, such as foraminifera (*e.g.*, Vance and Burton, 1999) and Fe-Mn (oxyhydr) oxides (*e.g.*, Bayon *et al.*, 2004), are commonly interpreted as indicating relative contributions of different water masses and associated changes in ocean circulation. The accuracy of conclusions gleaned from these sediment and seawater εNd records is however dependent on understanding the processes affecting the Nd concentration and isotopic composition during transport of Nd from rock to seawater *via* rivers and during sediment dissolution in the ocean (*e.g.*, Jeandel *et al.*, 2007).

Many studies have assumed that solutes released during dissolution have the same εNd composition as the bulk rocks being dissolved. However, riverine dissolved εNd values can be different from both the suspended load and the bedrock over which the river has flowed (Goldstein and Jacobsen, 1987; Tricca *et al.*, 1999; Andersson *et al.*, 2001; Rickli *et al.*, 2013). Additionally the rare earth element (REE) chemistry of sediment/soil leachates indicates that REE (including Sm and Nd) are mobile and can be fractionated during chemical weathering and diagenesis (*e.g.*, Bock *et al.*, 1994; Viers and Wasserburg, 2004). Goldstein and Jacobsen (1987) proposed that dissolved load εNd values are controlled by labile phases but direct evidence has been lacking. In this study we present εNd data on the dissolved load, stream suspended sediment and leachates (which access labile phases) of rock and glacial sediment samples in the same catchment to investigate the compositions and decoupling of these reservoirs.

We present data for an Arctic catchment (Svalbard, Supplementary Information) where the bedrock εNd and $^{87}Sr/^{86}Sr$ data were interpreted as a two component mixture between two sources: Proterozoic sediments derived from Greenlandic basement rocks and Carboniferous to Jurassic sediments derived from Siberian basalts (Hindshaw *et al.*, 2018). Due to recent glaciation, there has been negligible soil development which along with the large εNd range in the rocks exposed in the catchment (>12 epsilon units), the well-constrained field setting and its geographic location proximal to deep water formation, makes it an ideal site to evaluate the processes affecting εNd during river transport from terrestrial

1. Department of Earth Sciences, University of Cambridge, Downing Street, Cambridge, CB2 3EQ, UK
2. Department of Earth and Environmental Sciences, University of Michigan, 1100N. University Avenue, Ann Arbor, MI 48109, USA
* Corresponding author (email: ruth.hindshaw@gmail.com)

rock sources to the ocean. We find that similar to the well-established behaviour of radiogenic Sr (*e.g.*, Blum *et al.*, 1994), the dissolved εNd values are distinct from stream suspended sediments. Through sequential extractions of catchment rock and glacial sediment samples we demonstrate that dissolved εNd values are controlled by the most readily dissolved components, which are isotopically distinct from the bulk.

Decoupling Water Chemistry from Bulk Rock Compositions

The dissolved load (<0.22 µm) has higher εNd (2.0-5.5) and lower $^{87}Sr/^{86}Sr$ (0.020-0.028) values (Fig. 1a, Table S-2) compared to the corresponding stream suspended sediment samples (>0.22 µm; Hindshaw *et al.*, 2018). These differences result in an offset between the dissolved load Sr-Nd array and solid sample array (Fig. 1a), implying that the solid samples contain isotopically distinct phases that are preferentially weathered.

To investigate the compositions of the phases which are most labile and therefore likely to contribute to water chemistry, a range of rock and glacial sediment samples were leached (Supplementary Information, Haley *et al.*, 2008; Chen *et al.*, 2012). The εNd values of hydroxylamine hydrochloride (HH) and acetic acid (AA) leachates are always higher than the εNd values of the bulk sample (Fig. 1b, Table S-3).

The dissolved load samples define a linear trend bounded by the leachates from the three rock samples containing >1 % bulk Nd in the leachates (Table S-4). A mixing line can be fitted between HH leachate end members R1 and R3, which passes through the dissolved load samples (Fig. 1c), implying that the dissolved load composition is a mixture of these two labile end members. The chemical extraction procedure, which was developed to extract seawater Nd isotopes from authigenic phases in sediment cores (*e.g.*, Haley *et al.*, 2008), appears to target the same labile, end member phases as natural chemical weathering conditions.

The first end member is defined by the leachates from the shale samples R1 and R2 (Fig. 1b). Given that these shales were deposited in a deep water marine environment (Hindshaw *et al.*, 2018), this labile phase is likely an authigenic phase precipitated from seawater. To aid in identifying the source of Nd, we utilise rare earth element (REE) patterns (*e.g.*, Haley *et al.*, 2004; Supplementary Information). When normalised to the bulk REE pattern, the AA and HH leachates of R1 and R2 have a middle REE (MREE) enrichment (Fig. 2, Table S-5), which indicates the REE are hosted in authigenic phosphate minerals and/or Fe-Mn (oxyhydr)oxides (*e.g.*, Goldberg *et al.*, 1963; Sholkovitz *et al.*, 1999, Supplementary Information). The Sm/Nd ratios in the leachate samples (AA: 0.27-0.30; HH: 0.37-0.39) are higher than those of the bulk rock (0.19, typical for shale; McCulloch and Wasserburg, 1978) consistent with leaching of marine precipitates, as these phases preferentially incorporate Sm (Goldstein *et al.*, 1984).

The second end member is defined by the leachates from the sandstone sample (R3, Fig. 1b). The AA and HH leachates removed 91 % Ca and 88 % Sr respectively (Table S-4), with a Ca/Sr mass ratio of 325 (Veizer, 1983), strongly suggesting the presence of a carbonate phase. The sandstone leachates have a Sm/Nd mass ratio (0.20-0.21) typical for carbonates (~0.20, Hua *et al.*, 2013), and a high REE (HREE) enrichment (Fig. 2), typical for complexation with carbonate (*e.g.*, Byrne and Sholkovitz, 1996). This implies that Nd, like Sr, is hosted in the carbonate phase of this rock sample.

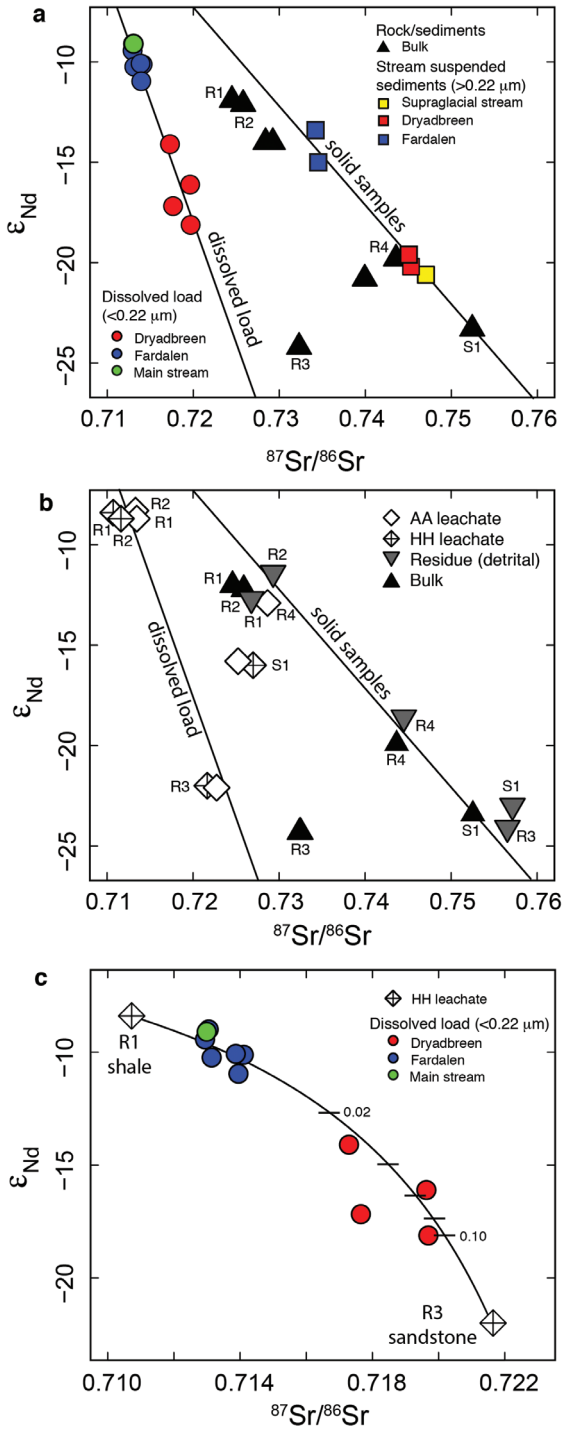

Figure 1 Dissolved (<0.22 µm) and solid samples (rock, sediment and stream suspended sediment) form distinct arrays in Sr-Nd space. **(a)** A linear regression is fitted for the dissolved samples ($r^2 = 0.93$, $p < 0.001$). The linear line for the solid samples is the mixing line between a Greenlandic ($^{87}Sr/^{86}Sr = 0.78059$, εNd = -37.1) and Siberian ($^{87}Sr/^{86}Sr = 0.70626$, εNd = -0.4) sediment source with identical Sr/Nd mass ratios (Hindshaw *et al.*, 2018). The four rock and one glacial sediment sample subjected to the leaching procedure are labelled. **(b)** The isotopic compositions of the leachates, residual and bulk samples. The dissolved load array is bound by leachates of the sandstone (R3) at one end and leachates of the shale samples (R1 and R2) at the other end. **(c)** The dissolved samples can be fitted with a mixing line between the HH leachate end members. The best fit line uses the concentration and isotopic values measured in R3-HH and R1-HH (Table S-3). The numbers on the mixing line refer to the mass fraction of the sandstone end member in the mixture. Error bars are smaller than symbol size.

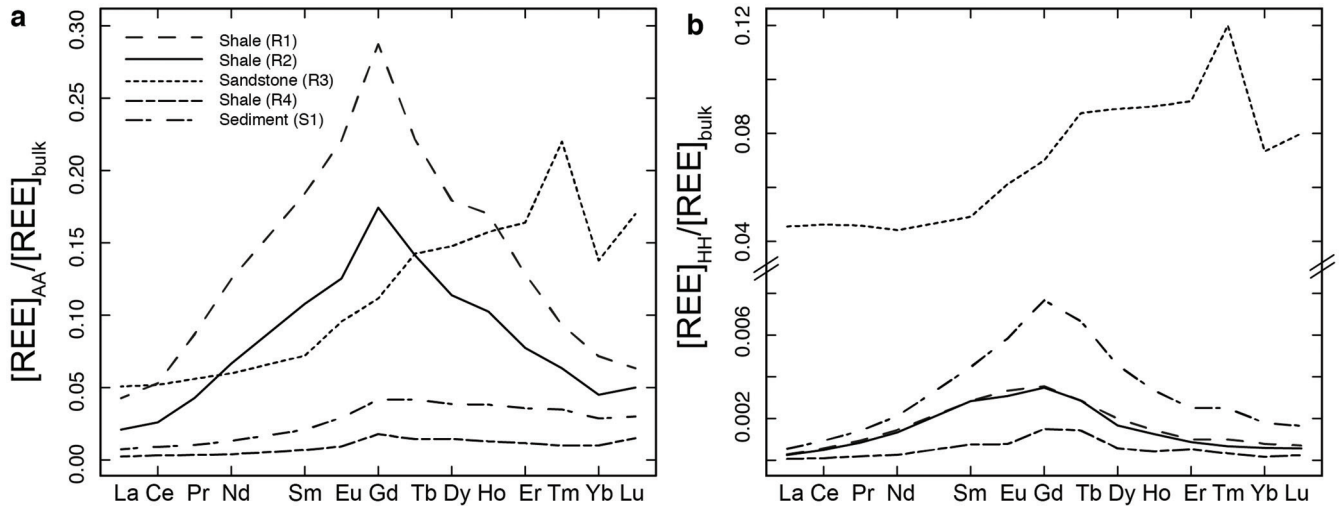

Figure 2 REE concentrations of the leachates normalised to bulk. **(a)** AA leach. **(b)** HH leach. REE concentrations are normalised against the bulk REE concentrations of the same sample. Note the scale break in **(b)**. The sandstone sample (R3) has a HREE enriched pattern for both leachates. Shale samples R1 and R2 have MREE enriched patterns for both leachates. REE data is reported in Table S-5.

In summary, εNd values of the dissolved load are distinct from those of stream suspended sediment sampled at the same time. We attribute this to the preferential leaching of two components found in sedimentary rocks in the catchment; 1) authigenic phosphates and/or Fe-Mn (oxyhydr)oxides, and 2) carbonate. Both phases have chemical and isotopic compositions distinct from the detrital silicate fraction (Fig. 1b).

Implications for Leaching an Isotopically Distinct Labile Phase

Sedimentary rocks contain a mixture of authigenic, detrital and biological components. The results from this study imply that in areas with extensive sedimentary rock cover, weathering of labile phases may dominate the riverine Nd flux, with two important implications. First, εNd measurements of bulk rock or the detrital silicate fraction will not represent the continental εNd input to ocean water masses. Second, analogous to $^{87}Sr/^{86}Sr$, εNd released to rivers and seawater will be controlled by the availability of (often) isotopically distinct labile phases *e.g.*, oxides. In weathering-limited regimes, where the availability of labile phases is not limited, εNd will be subject to environmental factors, such as discharge and temperature, which determine whether the dissolution of labile phases is promoted or suppressed (West *et al.*, 2005).

This has important implications for studies calculating budgets of seawater Nd isotopes relative to lithological sources, suggesting greater temporal and spatial variability. Using the Arctic Ocean as an example, where 49 % of the land drains shales (Amiotte Suchet *et al.*, 2003), we predict (Supplementary Information) that if a change in climatic or erosional conditions resulted in the weathering regime evolving from transport-limited, where the contribution of labile phases is negligible, to weathering-limited, where the dissolution of labile phases is dominant, then this would shift the εNd value of the ocean by 1 epsilon unit in just over 1τ (Nd residence time; Fig. S-2). This basic calculation only considers the dissolved load. However, if the proportion of sedimentary rock exposed to chemical weathering and the flux of stream suspended sediment were greater immediately after periods of glaciation (Vance *et al.*, 2009), then increased preferential weathering of labile phases from that sediment could occur in the marine environment, providing a climate-linked mechanism to alter the end member composition of water masses, independent of the source of Nd isotopes to the site of deep water formation, or of the location of deep water formation.

On long geological timescales, we suggest that if a fraction of the dissolved load was derived from a labile phase with a marine origin, then it could act as a "buffer" on seawater compositions. This would result in the geochemical decoupling between a labile sedimentary reservoir, which more readily exchanges with seawater due to rapid dissolution kinetics, and a silicate-bound reservoir, which maintains its composition set by crystallisation, plus radiogenic ingrowth through time. The leachates measured in this study have Sm/Nd ratios >20 % higher than the silicate fraction in the same sample (Table S-3), in agreement with literature values (Shaw and Wasserburg, 1985; Charbonnier *et al.*, 2012). If allowed to evolve 500 Myr, the εNd composition of the labile reservoir would become 1.5 epsilon units more radiogenic than the detrital silicate fraction due to ingrowth of ^{143}Nd (Supplementary Information). The exchange of this labile reservoir with seawater would result in seawater with a more radiogenic composition than the geological terranes that surround it, even in the absence of a volcanic fraction within marine sediment, which tends to contribute Nd preferentially to seawater (Pearce *et al.*, 2013; Wilson *et al.*, 2013). Exchange of εNd between seawater and labile phases during sediment recycling would cause the composition of terrestrial fine sediment to shift progressively further from bulk silicate rock towards higher εNd values over long geological timescales.

Acknowledgements

This project was funded by a Swiss National Science Foundation Fellowship for prospective researchers (PBEZP2-137335), a Marie Curie Intra-European Fellowship (PIEF-GA-2012-331501), and NERC Standard Grant NE/M001865/1. Fieldwork was supported by an Arctic Field Grant (219165/E10, The Research Council of Norway). RSH thanks the fieldwork team, Christina Larkin and Tom Williams for assistance with the leaching procedure and Greg de Souza for advice on oceanic box models. We wish to thank Catherine Jeandel, two anonymous reviewers and editor Liane Benning for their constructive comments that helped improve this manuscript.

Editor: Liane G. Benning

Additional Information

Supplementary Information accompanies this letter at http://www.geochemicalperspectivesletters.org/article1828.

Cite this letter as: Hindshaw, R.S., Aciego, S.M., Piotrowski, A.M., Tipper, E.T. (2018) Decoupling of dissolved and bedrock neodymium isotopes during sedimentary cycling. *Geochem. Persp. Let.* 8, 43–46.

References

Amiotte Suchet, P., Probst, J.-L., Ludwig, W. (2003) Worldwide distribution of continental rock lithology: Implications for the atmospheric/soil CO_2 uptake by continental weathering and alkalinity river transport to the oceans. *Global Biogeochemical Cycles* 17, 1038.

Andersson, P.S., Dahlqvist, R., Ingri, J., Gustafsson, Ö. (2001) The isotopic composition of Nd in a boreal river: A reflection of selective weathering and colloidal transport. *Geochimica et Cosmochimica Acta* 65, 521-527.

Bayon, G., German, C.R., Burton, K.W., Nesbitt, R.W., Rogers, N. (2004) Sedimentary Fe-Mn oxyhydroxides as paleoceanographic archives and the role of aeolian flux in regulating oceanic dissolved REE. *Earth and Planetary Science Letters* 224, 477-492.

Bayon, G., Burton, K.W., Soulet, G., Vigier, N., Dennielou, B., Etoubleau, J., Ponzevera, E., German, C.R., Nesbitt, R.W. (2009) Hf and Nd isotopes in marine sediments: Constraints on global silicate weathering. *Earth and Planetary Science Letters* 277, 318-326.

Blum, J.D., Erel, Y., Brown, K. (1994) $^{87}Sr/^{86}Sr$ ratios of Sierra Nevada stream waters: Implications for relative mineral weathering rates. *Geochimica et Cosmochimica Acta* 58, 5019-5025.

Bock, B., McLennan, S.M., Hanson, G.N. (1994) Rare earth element redistribution and its effects on the neodymium isotope system in the Austin Glen Member of the Normanskill Formation, New York, USA. *Geochimica et Cosmochimica Acta* 58, 5245-5253.

Byrne, R.H., Sholkovitz, E.R. (1996) Marine chemistry and geochemistry of the lanthanides. In: Gschneidner, Jr., K.A., Eyring, L. (Eds.) *Handbook on the Physics and Chemistry of Rare Earths. Vol. 23.* Elsevier, Oxford, 497-593.

Charbonnier, G., Pucéat, E., Bayon, G., Desmares, D., Dera, G., Durlet, C., Deconinck, J.-F., Amédro, F., Gourlan, A.T., Pellenard, P., Bomou, B. (2012) Reconstruction of the Nd isotope composition of seawater on epicontinental seas: Testing the potential of Fe-Mn oxyhydroxide coatings on foraminifera tests for deep-time investigations. *Geochimica et Cosmochimica Acta* 99, 39-56.

Chen, T.-Y., Frank, M., Haley, B. A., Gutjahr, M., Spielhagen, R.F. (2012) Variations of North Atlantic inflow to the central Arctic Ocean over the last 14 million years inferred from hafnium and neodymium isotopes. *Earth and Planetary Science Letters* 353-354, 82-92.

Goldberg, E.D., Koide, M., Schmitt, R.A., Smith, R.H. (1963) Rare-earth distributions in the marine environment. *Journal of Geophysical Research* 68, 4209-4217.

Goldstein, S.L., O'Nions, R.K., Hamilton, P.J. (1984) A Sm-Nd isotopic study of atmospheric dusts and particulates from major river systems. *Earth and Planetary Science Letters* 70, 221-236.

Goldstein, S.J., Jacobsen, S.B. (1987) The Nd and Sr isotopic systematics of river-water dissolved material: Implications for the sources of Nd and Sr in seawater. *Chemical Geology* 66, 245-272.

Haley, B.A., Klinkhammer, G.P., McManus, J. (2004) Rare earth elements in pore waters of marine sediments. *Geochimica et Cosmochimica Acta* 68, 1265-1279.

Haley, B.A., Frank, M., Spielhagen, R.F., Eisenhauer, A. (2008) Influence of brine formation on Arctic Ocean circulation over the past 15 million years. *Nature Geoscience* 1, 68-72.

Hindshaw, R.S., Tosca, N.J., Piotrowski, A.M., Tipper, E.T. (2018) Clay mineralogy, strontium and neodymium isotope ratios in the sediments of two High Arctic catchments (Svalbard). *Earth Surface Dynamics* 6, 141-161.

Hua, G., Yuansheng, D., Lian, Z., Jianghai, Y., Hu, H. (2013) Trace and rare earth elemental geochemistry of carbonate succession in the Middle Gaoyuzhuang Formation, Pingquan Section: Implications for Early Mesoproterozoic ocean redox conditions. *Journal of Palaeogeography* 2, 209-221.

Jeandel, C., Arsouze, T., Lacan, F., Téchiné, P., Dutay, J.-C. (2007) Isotopic Nd compositions and concentrations of the lithogenic inputs into the ocean: A compilation, with an emphasis on the margins. *Chemical Geology* 239, 156-164.

McCulloch, M.T., Wasserburg, G.J. (1978) Sm-Nd and Rb-Sr chronology of continental crust formation. *Science* 200, 1003-1011.

Pearce, C.R., Jones, M.T., Oelkers, E.H., Pradoux, C., Jeandel, C. (2013) The effect of particulate dissolution on the neodymium (Nd) isotope and Rare Earth Element (REE) composition of seawater. *Earth and Planetary Science Letters* 369-370, 138-147.

Piepgras, D.J., Wasserburg, G.J. (1980) Neodymium isotopic variations in seawater. *Earth and Planetary Science Letters* 50, 128-138.

Rickli, J., Frank, M., Stichel, T., Georg, R.B., Vance, D., Halliday, A.N. (2013) Controls on the incongruent release of hafnium during weathering of metamorphic and sedimentary catchments. *Geochimica et Cosmochimica Acta* 101, 263-284.

Shaw, H.F., Wasserburg, G.J. (1985) Sm-Nd in marine carbonates and phosphates: Implications for Nd isotopes in seawater and crustal ages. *Geochimica et Cosmochimica Acta* 49, 503-518.

Sholkovitz, E.R., Elderfield, H., Szymczak, R., Casey, K. (1999) Island weathering: river sources of rare earth elements to the Western Pacific Ocean. *Marine Chemistry* 68, 39-57.

Taylor, S.R., McLennan, S.M. (1985) *The continental crust: Its composition and evolution*. Blackwell Scientific, Boston, MA.

Tricca, A., Stille, P., Steinmann, M., Kiefel, B., Samuel, J., Eikenberg, J. (1999) Rare earth elements and Sr and Nd isotopic compositions of dissolved and suspended loads from small river systems in the Vosges mountains (France), the river Rhine and groundwater. *Chemical Geology* 160, 139-158.

Vance, D., Burton, K. (1999) Neodymium isotopes in planktonic foraminifera: a record of the response of continental weathering and ocean circulation rates to climate change. *Earth and Planetary Science Letters* 173, 365-379.

Vance, D., Teagle, D.A.H., Foster, G.L. (2009) Variable Quaternary chemical weathering fluxes and imbalances in marine geochemical budgets. *Nature* 458, 493-496.

Veizer, J. (1983) Chemical diagenesis of carbonates: theory and application of trace element technique. In: Arthur, M.A., Anderson, T.F., Kaplan, I.R., Veizer, J., Land, L.S. (Eds.) *Stable isotopes in sedimentary geology. Society of Economic Paleontologists and Mineralogists Short Course Notes Vol. 10.* SEPM Society for Sedimentary Geology, Dallas, USA, 3-1-3-100.

Viers, J., Wasserburg, G.J. (2004) Behavior of Sm and Nd in a lateritic soil profile. *Geochimica et Cosmochimica Acta* 68, 2043-2054.

West, A.J., Galy, A., Bickle, M. (2005) Tectonic and climatic controls on silicate weathering, *Earth and Planetary Science Letters* 235, 211-228.

Wilson, D.J., Piotrowski, A.M., Galy, A., Clegg, J.A. (2013) Reactivity of neodymium carriers in deep sea sediments: Implications for boundary exchange and paleoceanography. *Geochimica et Cosmochimica Acta* 109, 197-221.

Geochemical Perspectives Letters

Decoupling of dissolved and bedrock neodymium isotopes during sedimentary cycling

R.S. Hindshaw, S.M. Aciego, A.M Piotrowski, E.T. Tipper

Supplementary Information

The Supplementary Information includes:

- 1. Sampling and Analytical Methods
- 2. Precipitation Correction
- 3. Further Details on the Identification of the Source of Labile Sr and Nd in Rocks R1, R2 and R3
- 4. Rough Estimate of the Potential Magnitude of εNd Variation by Changing the Weathering Regime
- 5. Estimate of the Magnitude of Divergence of εNd in Detrital and Labile pools
- Tables S-1 to S-5
- Figures S-1 to S-4
- Supplementary Information References

1. Sampling and Analytical Methods

1.1 Field sample collection

We studied two small (< 4 km^2) catchments located in the Palaeogene sedimentary Central Basin of Svalbard, which covers 8 % of the archipelago (Fig. S-1). The sedimentary formations exposed in the catchments are from the Van Mijenfjorden group which is Paleocene to Eocene in age (66 - 33.9 Ma) and contains sandstones, siltstones and shale.

The three youngest formations are exposed in the two catchments (Major *et al.*, 2000) and were sourced from erosion of the uplifted West Spitsbergen Fold and Thrust Belt whose formation is linked to rifting of the North Atlantic and the separation of Svalbard from Greenland (Helland-Hansen, 1990; Müller and Spielhagen, 1990). The sediments were derived from two isotopically and geochemically distinct sediment sources which mixed during the Mesozoic. One end-member is Proterozoic sediments derived from Greenlandic basement rocks and the second end-member is Carboniferous to Jurassic sediments derived from Siberian basalts (Hindshaw *et al.*, 2018). The Eocene sediments comprise a regressive sequence with (from oldest to youngest) the Frysjaodden Formation comprising fine-grained shales deposited offshore in an open basin; Battfjellet Formation comprising shallow marine sandstone; and Aspelintoppen Formation comprising continental deposits (Helland-Hansen, 1990; Müller and Spielhagen, 1990). No volcanic phases are present in these sedimentary formations though bentonite (a clay mineral), derived from the alteration of volcanic ash, is present (Schlegel *et al.*, 2013).

Water and suspended sediment samples from the Dryadbreen and Fardalen streams (Fig. S-1) were sampled twice a day from 14th to 18th June 2012 and from 25th July to 3rd August 2012. The number of days sampled corresponds to approximately 20 % of the melt-season (Yde *et al.*, 2008). The two rivers were sampled just before they joined the main valley river. For Dryadbreen this was approximately 1 km from the front of the glacier. The main valley river (Fig. S-1, green point) was sampled after the confluence with the stream from Fardalen, but before the confluence with the stream from Dryadbreen. Temperature and pH were measured *in situ* (Hanna HI 98160 pH meter).

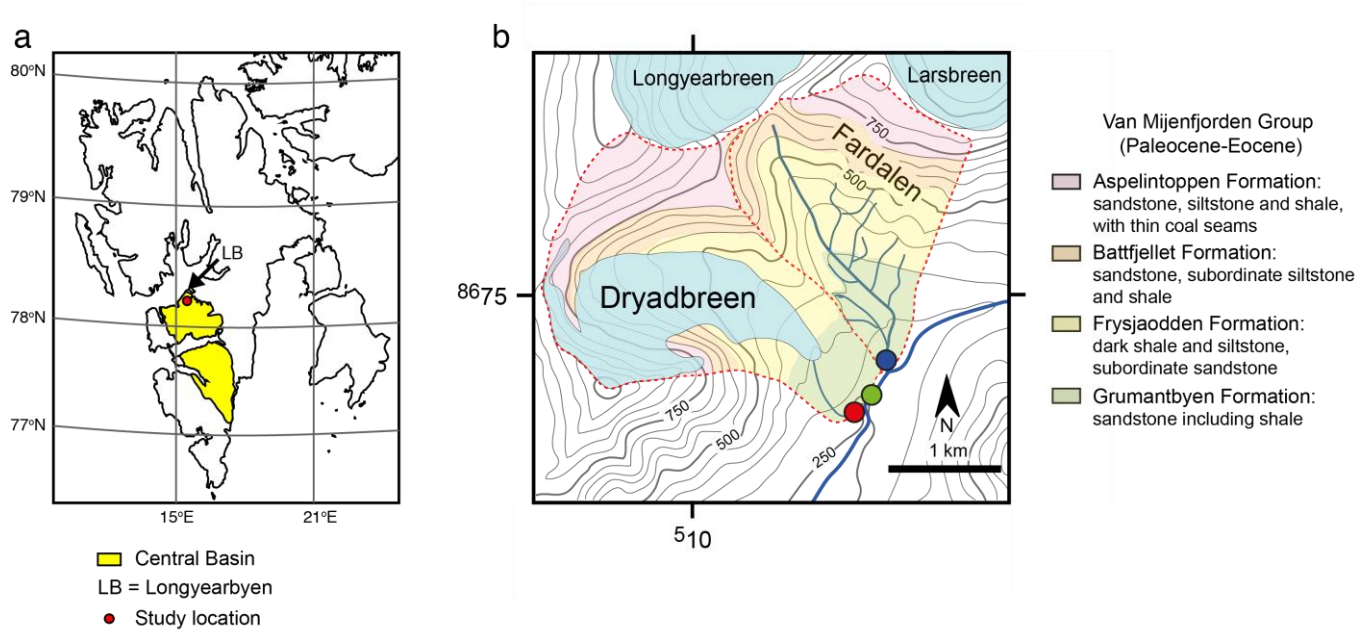

Figure S-1 Sample location maps. **(a)** Map of Svalbard indicating the extent of the Palaeogene Central Basin. The location of the study area in relation to Longyearbyen (the main settlement) is also indicated. **(b)** Topographic map of the catchments projected in universal transverse Mercator World Geodetic System (WGS 84) zone 33X with contours displayed at 50 m intervals and with geological information superimposed. Glaciers are highlighted in light blue and the red dashed lines demarcate the catchment boundaries. Dryadbreen is on the left and Fardalen on the right. The coloured circles indicate where the water samples (dissolved load and stream suspended sediments) were collected: Main stream (green circle), Fardalen (blue circle) and Dryadbreen (red circle). Figure modified from Hindshaw *et al.* (2016a).

The water sampling procedures for major ion chemistry are described in Hindshaw *et al.* (2016b). For strontium, a 1 L 0.22 µm filtered water sample was collected from each catchment every other day. This water sample was acidified to pH 2 with single-distilled concentrated HNO_3. For neodymium, water samples were collected following the procedure outlined in Arendt *et al.* (2015). A pre-cleaned 15 L plastic water carrier was filled with 0.22 µm filtered water (filtered using a polycarbonate vacuum filtration unit connected to a hand pump) then 7 mL 9 M HCl was added to the water followed by 3 mL of a pre-cleaned iron solution ($FeCl_3.6H_2O$ in 3 M HCl), resulting in an iron concentration of 15 mg/L. The mixture was shaken and after 10 min, 10 mL NH_4OH was added, raising the pH to approximately 8-9 and inducing iron precipitation. After 48 h of settling the bulk of the supernatant was gently poured off and the remaining solution was transferred to a 1 L bottle for transport from the field. In the laboratory, the remaining liquid was removed after centrifugation and the solid was digested in 1 mL 9 M HCl, dried down and taken up in 10 mL 12 M HCl.

The stream suspended sediment (>0.22 µm) deposited on nylon filter papers during filtration of the water samples was retrieved by washing the filter paper with deionized water and then freeze drying the sample. The solid was prepared for analysis using the same procedure described in section 1.2 for the residual fraction of the leaching procedure.

In this study we use the term "dissolved" for the <0.22 µm fraction in the knowledge that this phase will also contain colloidal material and that the true dissolved phase will likely have a distinct REE pattern (Viers *et al.*, 2004; Ilina *et al.*, 2013; Merschel *et al.*, 2017). However, colloidal material is derived the same ultimate source as the truly dissolved fraction, i.e. the colloidal fraction was dissolved before it became complexed. We therefore assume that the isotopic composition of the dissolved and colloidal fractions are the same and this is supported by measurements (Ilina *et al.*, 2013).

1.2 Leaching procedure

In order to separate out potential labile phases we applied a leaching procedure used in marine sciences (*e.g.*, Chester *et al.*, 1967;

Gutjahr *et al.*, 2007; Wilson *et al.*, 2013) to separate out the authigenic (when sediment deposition occurs in the ocean this will, by definition, be marine precipitates) from the detrital component of the sediment. The first two steps of this procedure are designed to target carbonates and authigenic minerals respectively (Wilson *et al.*, 2013). Five samples were selected which covered the range of $^{87}Sr/^{86}Sr$ and εNd isotopic compositions observed in the bulk solid samples (Hindshaw *et al.*, 2018). The five samples chosen were R03 (lithic sandstone), R04 and G (frost-shattered shale pieces), D (sediment, surface of glacier) and R01 (shale rock). These samples have been renamed for this study (Table S-1) to clearly distinguish between rock (R) and sediment (S) samples as follows: R01 → R1, G → R2, R03 → R3, R04 → R4 and D → S1.

Table S-1 Summary of the solid samples analysed in this study.

Solid Sample	Sample label in Hindshaw *et al.*, 2018	Description	AA/HH leaching procedure
R1 and R2	R01 and G	Shale pieces from the Frysjaodden Formation	yes
R3	R03	Lithic sandstone from the Aspelintoppen Formation	yes
R4	R04	Shale rock from the surface of the glacier	yes
S1	D	Sediment from the surface of the glacier	yes
Stream suspended sediment	20120617D, 20120729D, 20120618F and 20120726F	>0.22 μm stream suspended sediment	no

Approximately 8 g of sediment was added to a 50 mL centrifuge tube and about 25 mL of 0.47 M acetic acid buffered with 1 M sodium acetate (AA) was added. Samples were shaken overnight, centrifuged and the supernatant removed. The residual sediment was washed with MQe water (18.2 Ω) and then about 25 mL of a 0.005 M hydroxylamine hydrochloride – 2.6 M acetic acid mixture (HH) was added. This reagent is more dilute than commonly used in order to avoid leaching clay minerals (Haley *et al.*, 2008; Chen *et al.*, 2012). Samples were shaken for 1 h, centrifuged and the supernatant removed. The supernatant samples were centrifuged again and the top portion transferred to teflon beakers to dry down. The dried leachate was then digested in concentrated HNO_3 and then taken up in 2 % HNO_3 in preparation for analysis. The residue left over from the 0.005 M HH leach was further leached with 0.02 M HH to ensure only detrital phases remained. The residue was washed in water, dried, and then approximately 100 mg of material was ashed at 950 °C for 120 minutes. The sample was then digested in a mixture of concentrated hydrofluoric and nitric acids and repeatedly dried down and re-dissolved in 6 M HCl. In the final step, the dried down sample was re-dissolved in 2 % HNO_3.

1.3 Element concentration analysis

Trace element concentrations in water samples (including Sr, Rb, Sm and Nd) were measured on an inductively coupled plasma mass spectrometer (ICP-MS, Element, Thermo, University of Cambridge). Major element concentrations in leachate and residue samples were measured by ICP-OES (Agilent Technologies 5100, University of Cambridge) and trace element concentrations were measured by quadrupole ICP-MS (Perkin Elmer 63 Nexion 350D, University of Cambridge). Data on the accuracy and precision are reported in Hindshaw *et al.* (2018).

1.4 Isotope analysis

The procedure used to separate Nd from a stream water sample matrix is described in Arendt *et al.* (2015) and employs 4 different columns. The first column separates U from high field strength elements (HFSE) and rare earth elements (REE). Neodymium is subsequently separated from the HFSE-REE mixture by an additional three columns. Neodymium from leachate and residue samples was separated by a two-column procedure (Piotrowski *et al.*, 2009).

Neodymium ($^{143}Nd/^{144}Nd$) isotope ratios in water samples were measured on a Triton PLUS (Thermo Scientific, University of Michigan) thermal ionisation mass spectrometer (TIMS) (Arendt *et al.*, 2015). Based on Nd concentration measurements (Table S-2), the 15 L water samples contained 36 – 1600 ng Nd. The combined co-precipitation and column chemistry procedure had a yield of 90 % (Arendt *et al.*, 2015), therefore we calculate the final amount of Nd recovered to be 32 – 1440 ng. Half of this amount i.e. >16 ng was loaded in a concentrated mixture of 3 M HCl and 3 M HNO_3 onto degassed double rhenium filaments. Data acquisition was comprised of 200 measurements with a 4 s integration time.

Leachate and residue samples were run on a Neptune multi-collector ICP-MS (Thermo, University of Cambridge) at 100 ppb using a wet plasma technique with a double-pass spray chamber. Each measurement comprised 30 cycles with 10 s integration. Samarium interferences were monitored by measuring mass 149. No interferences were detected and oxides were monitored during tuning to ensure they were well below 0.5% of the beam size. The exponential law was applied to correct for instrument mass fractionation and all $^{143}Nd/^{144}Nd$ ratios were normalised to $^{146}Nd/^{144}Nd = 0.7219$. The mean of $^{143}Nd/^{144}Nd$ long-term measurements of 10 ng aliquots of JNdi-1 by TIMS over the period of this study was 0.512101 ± 0.000030 (εNd -10.48 ± 0.58, 2SD, n=61) (Arendt *et al.*, 2015), which is in agreement with the accepted value of 0.512115 (Tanaka *et al.*, 2000). The mean of JNdi-1 on

the Neptune was 0.512037 ± 0.000034 (2SD, n=25) and samples were bracketed by standards in order to correct for the offset with the accepted JNdi-1 value. The USGS shale standard SCo-1 was measured and the $^{143}Nd/^{144}Nd$ value was 0.512115 ± 0.000031 (n=2, 2SD) in agreement with a previously published value of 0.512117 ± 0.000010 (n=20, 2σ, Krogstad *et al.*, 2004). In this study neodymium ratios are reported as deviations in parts per ten thousand (εNd) relative to the chondritic uniform reservoir (CHUR, $^{143}Nd/^{144}Nd$ = 0.512638, Jacobsen *et al.*, 1980).

Strontium in water samples analysed for Nd was separated from matrix elements using the procedure outlined in Aciego *et al.*, 2009. Strontium isotope ratios ($^{87}Sr/^{86}Sr$) in water samples were measured on a Triton PLUS TIMS (Thermo Scientific, University of Michigan) (Stevenson *et al.*, 2016). The radiogenic strontium isotopic compositions of the remaining water samples (those not analysed for Nd) were measured on a VG Sector 54 solid source mass-spectrometer using triple-collector dynamic algorithm at the University of Cambridge (Chapman *et al.*, 2015). For both methods, approximately 250 ng Sr was loaded in nitric form together with 1 µL of tantalum phosphate activator solution onto degassed single rhenium filaments. Data acquisition was comprised of 400 measurements with a 4 s integration time. Leachate and residue samples were run on a Neptune MC-ICP-MS (Thermo, University of Cambridge) at 50 ppb using an APEX sample introduction system. Each measurement comprised 30 cycles with 8 s integration. For all measurements, ^{85}Rb was monitored to correct for rubidium interferences on ^{87}Sr and Neptune data were additionally corrected for Kr interferences by measuring ^{83}Kr. The exponential law was applied to correct for instrument mass fractionation and all $^{87}Sr/^{86}Sr$ ratios were normalised to $^{86}Sr/^{88}Sr$ = 0.1194. Long-term measurements of NBS 987 gave $^{87}Sr/^{86}Sr$ values of 0.710267 ± 20 (n=100) on the Triton, 0.710266 ± 16 (n=90) on the VG Sector 54 and 0.710257 ± 24 (n=27) on the Neptune. Measurements of seawater gave values of 0.709193 ± 9 (n=3) on the VG Sector 54 and 0.709183 ± 26 (n=10) on the Neptune, which are within error of the accepted value of 0.709179 ± 8 (Mokadem *et al.*, 2015).

2. Precipitation Correction

External inputs including rain, snow and soluble dust can be important sources of solutes to rivers. The following equation was used to correct measured $^{87}Sr/^{86}Sr$ values for precipitation inputs:

$$^{87}Sr/^{86}Sr^{*} = \frac{^{87}Sr/^{86}Sr_r.Sr_r-((Sr/Cl)_{snow}.Cl_r).^{87}Sr/^{86}Sr_{snow}}{Sr_r-(Sr/Cl)_{snow}.Cl_r} \quad \text{Eq. S-1}$$

where $^{87}Sr/^{86}Sr^{*}$ is the meteorological precipitation corrected Sr isotope ratio, 'r' denotes parameters measured in the river and 'snow' refers to the average of the two measured snow samples (Table S-2). The precipitation corrected isotope ratios for the water samples differ by a maximum of 4 ppm from the uncorrected values, which is well within analytical uncertainty. Neodymium concentrations measured in snow samples span the range of Nd concentrations measured in river water (Table S-2), and could potentially be a major source of Nd to the river. If external inputs were dominant, then both streams would be expected to have similar εNd values and show no relationship with $^{87}Sr/^{86}Sr$ values. This is not observed, and is inconsistent with the observed coherency in the Sr and Nd isotopic composition of the water samples. Furthermore, the water data is consistent with weathering sources from local rocks, and an isotopically distinct third end-member is not required (Fig. 1c).

3. Further Details on the Identification of the Source of Labile Sr and Nd in Rocks R1, R2 and R3

The buffered acetic acid (AA) leach is traditionally used to target carbonate phases in sediments, as these are often the most readily dissolved component (Tessier *et al.*, 1979). However, if present, some Fe-oxides and phosphates will also be dissolved as well as ions that are adsorbed onto mineral surfaces or are present in exchangeable sites (Chester and Hughes, 1967). The 0.005 M HH leach is a non-quantitative leach designed to extract the seawater isotope signal from authigenic Fe-Mn oxyhydroxide coatings in sediments without attacking clay minerals or dissolving detrital material (Haley *et al.*, 2008; Chen *et al.*, 2012; Blaser *et al.*, 2016). Al concentrations (all concentrations reported relative to the initial weight of the bulk sample, Table S-3) are negligible in both the AA and HH leachates of these three rock samples (< 100 mg kg^{-1}) confirming that the clay mineral structure has remained intact.

Rock sample R3 is a lithic sandstone (litharenite) derived from the Aspelintoppen Formation which contains continental deposits, likely deposited in a fluvial or deltaic environment (Helland-Hansen, 1990; Müller and Spielhagen, 1990). This sample contains 10 % calcite (measured by XRD) and, as outlined in the main text, the major element chemistry (Tables S-3, S-4) and Ca/Sr ratio of the AA and HH leachates is consistent with the removal of carbonate. This carbonate could be marine or pedogenic in origin. The Ca/Sr mass ratios of the R3 leachates (300-360) are consistent with detrital carbonates (>200, Channell *et al.*, 2012). Further, the measured $\delta^{13}C$ and $\delta^{18}O$ values of the carbonate in R3 are -12.4 ‰ PDB and -24.9 ‰ PDB, respectively. These values are not compatible with carbonate precipitated from Paleozoic seawater as there is no indication of seawater $\delta^{13}C_{carb}$ values below -

5 ‰ during this time period (Saltzman and Thomas, 2012). Rather, these C and O isotope values are consistent with soil (pedogenic) carbonate, where the $\delta^{18}O$ is set by local meteoric water and $\delta^{13}C$ is set by soil CO_2 (Cerling, 1984; Zamanian *et al.*, 2016), suggesting that the carbonate formed on land and was then eroded to form detrital carbonate in the subsequently forming sedimentary rock. The REE pattern and Sm/Nd ratio of the sandstone leachates are consistent with carbonate (Fig. 2, Table S-5), suggesting that Nd is also associated with carbonate. Carbonates typically have low REE concentrations (Shaw and Wasserburg, 1985) but non-biogenic carbonates (e.g. pedogenic) can have elevated Nd concentrations (Violette *et al.*, 2010; Blaser *et al.*, 2016).

Rock samples R1 and R2 are derived from the Frysjaodden Formation, which was deposited in a deep marine environment during a period straddling the Paleocene-Eocene boundary. We therefore expect the extraction procedure to leach labile phases formed in the marine environment during that time period. In the AA leach, P concentrations are low (2.3-2.4 mg kg^{-1}) compared to the HH leach (54-64 mg kg^{-1}, Table S-3) despite phosphate being readily dissolved in dilute acetic acid (Ohr *et al.*, 1994). Additionally, Ca concentrations were below the detection limit in the HH leach suggesting that it is unlikely a Ca-phosphate phase (e.g. apatite) was leached. However, Fe and Mn concentrations in the AA leachate were a factor of 10 greater than P concentrations (23-46 mg kg^{-1} and 33-74 mg kg^{-1} respectively, Table S-3), suggesting that Fe-Mn-oxides are the dominant labile phase being leached. We observe a MREE enrichment in both the AA and HH leachates of R1 and R2. MREE enrichments are common in phosphate minerals (e.g. Hannigan *et al.*, 2001; Tricca *et al.*, 1999; Aubert *et al.*, 2001) and are also observed in Fe-Mn oxyhydroxide coatings (e.g. Goldberg *et al.*, 1963; Johannesson and Zhou, 1999; Haley *et al.*, 2004), thus the MREE pattern alone cannot distinguish between these two phases. Similarly, the elevated Sm/Nd ratio in the AA and HH leachates (0.27-0.39) compared to the parent rock (0.19) does not uniquely identify the source of Nd, as both phosphate minerals and Fe-Mn oxyhydroxides exhibit elevated Sm/Nd ratios compared to the bulk parent sample. For example, an apatite sample had a Sm/Nd ratio of 0.48 compared to 0.24 in the bulk granite (Aubert *et al.*, 2001) and the average Sm/Nd from an extraction targeting Fe-Mn oxyhydroxide phases in clastic sedimentary rock samples was 0.33 compared to 0.22 in the bulk rocks (Johannesson and Zhou, 1999). Nevertheless, based on major element chemistry, a Fe-Mn oxyhydroxide source appears more likely than a phosphate source of Nd for R1 and R2.

4. Rough Estimate of the Potential Magnitude of εNd Variation by Changing the Weathering Regime

In this section we apply a very simplified model to assess whether a change in ocean εNd would be observed if the terrestrial weathering regime changed. We assume a single well-mixed box to represent the surface layer of the Arctic Ocean. In response to a change in input flux, the evolution of a well-mixed reservoir toward a new steady-state can be modelled by combining the washing out of the old state (Eqs. S-2 and S-3) and the ingrowth of the new state (Eqs. S-4 and S-5).

$$\frac{dM}{dt} = -kM \qquad \text{Eq. S-2}$$

$$M(t) = M_0 e^{kt} \qquad \text{Eq. S-3}$$

$$\frac{dM}{dt} = J - kM \qquad \text{Eq. S-4}$$

$$M(t) = J/k(1 - e^{kt}) \qquad \text{Eq. S-5}$$

where M is the quantity of material in the reservoir, t is time, k is the kinetic constant and J is the input flux. At equilibrium, the residence time, $\tau = 1/k$. Additionally, as $t \rightarrow \infty$, M in Equation S-5 will tend to J/k, i.e. $M_\infty = J/k$. Substituting into Equations S-3 and S-5, and combining, we obtain:

$$M(t) = M_0 e^{-t/\tau} + M_\infty(1 - e^{-t/\tau}) \qquad \text{Eq. S-6}$$

An identical form of Equation S-6 can be obtained for an isotope ratio instead of a mass, giving:

$$\varepsilon Nd(t) = \varepsilon Nd_0 e^{-t/\tau} + \varepsilon Nd_\infty(1 - e^{-t/\tau}) \qquad \text{Eq. S-7}$$

where εNd_0 is the initial Nd isotopic composition of the surface layer of the Arctic Ocean and εNd_∞ is the new isotopic composition once the system has re-gained steady state. The input of Nd to the surface layer of the Arctic Ocean is comprised of dissolved load from rivers, dust and boundary exchange processes, which ultimately derive from river sediments. A recent study in the estuary of

the Amazon river suggested that river sediments likely contribute significantly to the global marine dissolved Nd budget (Rousseau *et al.*, 2015) and the same labile phases are likely to be released in both terrestrial and marine environments. The Arctic Ocean has extensive continental shelf areas where particulate dissolution in seawater has been shown to impact seawater εNd (Laukert *et al.*, 2017).

For the purposes of this model, we assume that the initial state is a transport limited weathering regime where dissolved load εNd is identical to suspended load εNd and the new state is kinetically limited where isotopically distinct labile phases dominate fluxes. 49% of the area draining into the Arctic Ocean is shale (Amiotte Suchet *et al.*, 2003) and therefore likely to contain the labile phases identified in this study. If 49 % of the input to the surface layer of the Arctic Ocean is shifted by 3 epsilon units (the average offset of R1, R2 and R3 leachates from bulk rocks), then the new steady state input flux will be $\varepsilon Nd_0 + 1.47$. The temporal evolution of the reservoir as a result of this perturbation is depicted in Figure S-2. This simple model only considers the dissolved load and does not take into account changes in sediment flux. An increase in total sediment flux would likely increase the amount of Nd released from labile phases contained in the sediment to the marine environment and impact the rate of change of ocean εNd.

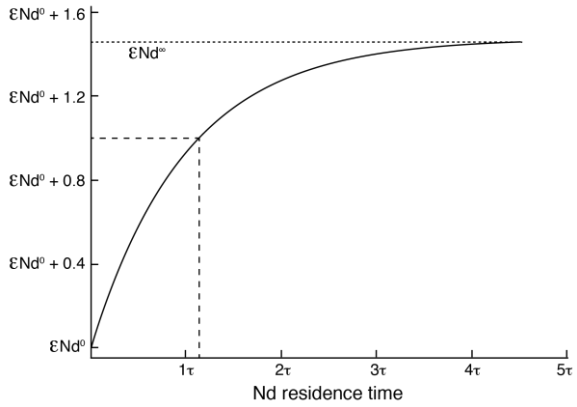

Figure S-2 Change in εNd in a well-mixed reservoir *e.g.* the surface layer of the Arctic Ocean with time after a 1.47 epsilon unit change in the input flux (see text for details). A 1 epsilon unit change could be observed after just over 1 residence time.

4.1 Effect of grain-size variations on εNd values of river sediments

The radiogenic Nd isotopic composition of river sediments appears to be minimally affected by sediment grain-size in the majority of rivers studied to date (Garçon *et al.*, 2013; Bayon *et al.*, 2015). In some large rivers, grain-size effects have been observed and this has been attributed to an enrichment of basaltic and volcanogenic particles in the fine particulate fraction and enrichment of crystalline sources in the coarse fraction (Garçon *et al.*, 2014; Bayon *et al.*, 2015). Because the former lithologies tend to have higher εNd values than the latter, this leads to an offset in the εNd of fine and coarse sediments (Garçon *et al.*, 2014; Bayon *et al.*, 2015). The fate of sedimentary rocks depends on the other lithologies present: sedimentary rocks will be enriched in the fine fraction compared to crystalline rocks but not compared to basalt (Garçon *et al.*, 2014; Bayon *et al.*, 2015). The fine sediment input to the Arctic Ocean is unlikely to be significantly enriched in basalt as basalt only accounts for 8.3 % of the area draining into the ocean and shales, which are fine-grained, account for 49.4 % of the area (Amiotte Suchet *et al.*, 2003). Fine sediments could have a disproportionate effect on the εNd value of the surface layer of the ocean as they travel further before settling, increasing the likelihood that the labile phase dissolves, adding radiogenic Nd to the surface layer.

5. Estimate of the Magnitude of Divergence of εNd in Detrital and Labile pools

The equation for radioactive decay for the Sm-Nd system is given by:

$$\frac{^{143}Nd}{^{144}Nd} = \left(\frac{^{143}Nd}{^{144}Nd}\right)_0 + \left(\frac{^{147}Sm}{^{144}Nd}\right)\lambda_{147}t \qquad \text{Eq- S-8}$$

where λ_{147} is 6.54×10^{-12} yr^{-1}. For the purposes of this model the initial $^{143}Nd/^{144}Nd$ ratio is taken to be 0.512638 (CHUR) to give an initial εNd value of 0. Assuming that ^{147}Sm is 0.150*[Sm] (de Laeter *et al.*, 2000) and ^{143}Nd is 0.238*[Nd] (de Laeter *et al.*, 2000), then the $^{147}Sm/^{144}Nd$ ratio for the detrital fraction is 0.105 (based on average Sm/Nd ratio of 0.166 in the detrital fractions, Table S-3) and 0.129 in the labile fraction (based on the average Sm/Nd ratio of 0.205 in the two R3 leachates, Table S-3). The evolution of the two

pools with time is given in Figure S-3a, and a 1.6 epsilon unit difference will arise after 0.5 Ga (Fig. S-3b). This is a minimum estimate as the Sm/Nd ratios of the leachates from the shale samples (R1 and R2) are higher (up to 0.39, Table S-3).

The potential for a decoupling between the Nd isotopic composition of bulk and clay-sized sediments was previously reported (Bayon *et al.*, 2015) and was attributed to the processes outlined in section 4.1 whereby radiogenic basalt particles from mixed lithology catchments become enriched in the fine-fraction. Thus, the 1.5 εNd difference observed between the clay and silt fractions of Mississippi river sediments (a basin mainly comprised of marine sedimentary formations) was attributed to ancient episodes of basalt weathering (Bayon *et al.*, 2015). However, in this study we have outlined an alternative mechanism that could account for the Mississippi results: preferential weathering of mineral phases derived from marine precipitates. This process could be significant in any basin containing sedimentary rocks deposited in a marine setting.

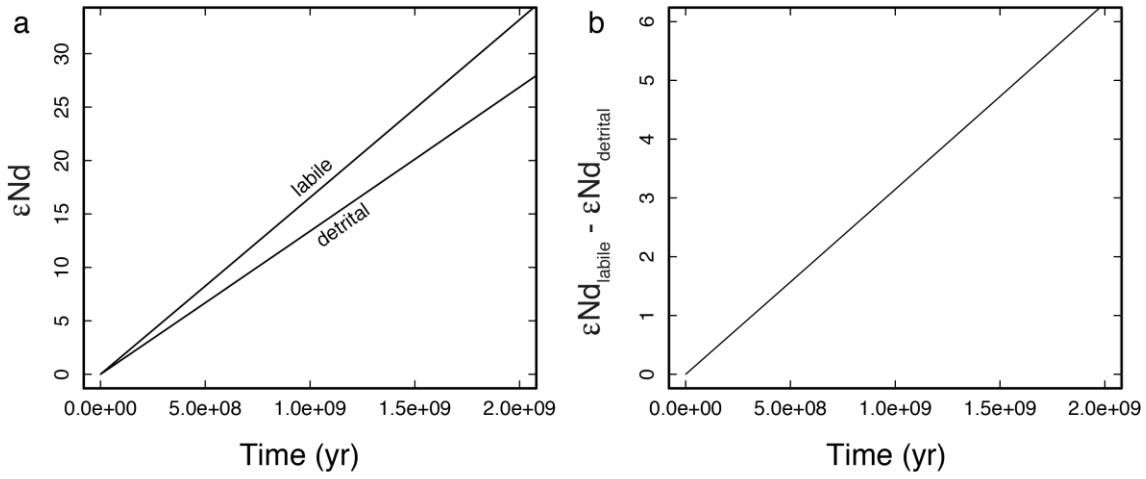

Figure S-3 Divergence of εNd in labile and detrital fractions over time (**a**, see text for details). A 1.5 epsilon unit change could be observed after 0.5 Gyr (**b**).

Supplementary Figure

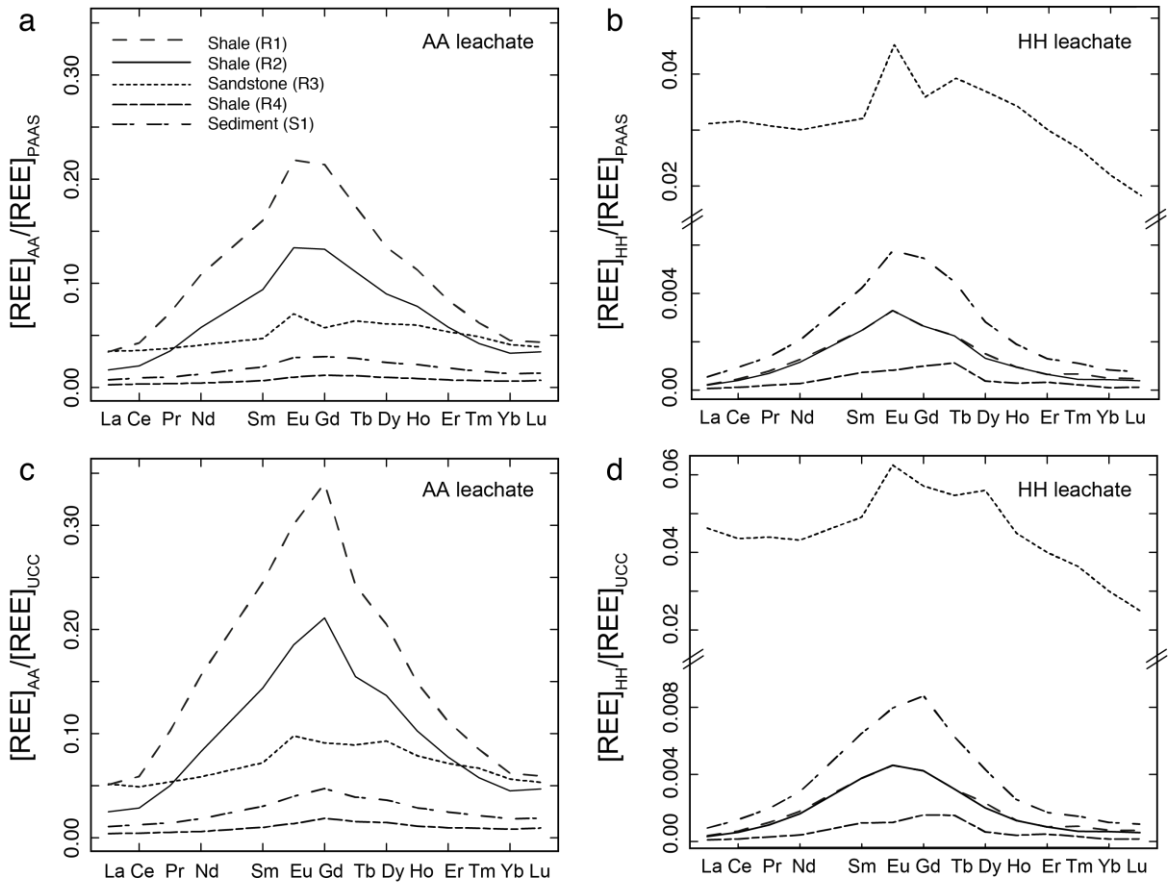

Figure S-4 Normalised REE patterns. REE concentrations of the AA (**a,c**) and HH (**b,d**) leachates normalised to Post-Archean Australian Shale (PAAS, **a,b**) and Upper Continental Crust (UCC, **c,d**). Note the scale break in **b** and **d**. UCC and PAAS values are taken from McLennan (2001) and Pourmand *et al.* (2012), respectively.

Supplementary Tables

Table S-2 Major element, trace element and Sr and Nd radiogenic isotopic compositions of dissolved load (<0.22 µm) samples. Only part of the major element data is reported, full data can be found in Hindshaw *et al.* (2016b).

Sample	Time	pH	Ca	Mg	Na	Cl	SO_4	HCO_3	Mn	Ba	Sr	Rb	Nd	Sm	$^{87}Sr/^{86}Sr$	2SD[1]	εNd	2SE
(YYYYMMDD)	(local)		µmol L^{-1}						µg L^{-1}			ng L^{-1}				(ppm)		
Dryadbreen (glaciated)																		
20120615D	11:26	6.91	125	124	188	208	113	263	11.6	9.1	24.5	166	8.9	2.2	0.717654	16	-17.18	0.08
20120617D	10:20	5.94	96	93	160	190	75	195	9.6	8.4	18.6	171	7.4	1.3	0.717291	40	-14.10	0.10
20120725D	10:10	6.76	108	100	85	40	94	315	40.7	11.8	24.1	226	3.5	1.3	0.719634	14	-16.11	0.12
20120727D	09:00	7.18	141	131	107	42	137	372	40.1	13.2	31.4	165	2.7	0.6	0.719376	5	n.d.	n.d.
20120729D	08:45	6.34	115	106	94	36	110	284	26.1	9.6	24.4	131	2.4	1.0	0.719692	8	-18.12	0.14
20120731D	08:37	6.91	144	135	111	44	141	349	24.6	12.2	29.8	237	113	26.7	0.719535	9	n.d.	n.d.
20120801D	16:17	6.86	109	98	80	37	90	212	29.6	17.8	22.5	139	3.3	0.8	0.719960	17	n.d.	n.d.
20120802D	08:50	6.89	137	125	131	53	124	299	20.9	19.3	27.3	293	32.5	6.9	0.719790	26	n.d.	n.d.
Main stream																		
20120613MS	15:10	7.53	142	174	272	213	291	n.d.	88.4	10.1	38.8	237	107	28.3	0.712991	21	-9.10	0.10
Fardalen (unglaciated)																		
20120614F	10:26	7.37	213	253	323	226	461	130	132	15.6	54.6	273	69.5	19.0	0.713054	53	n.d.	n.d.
20120616F	10:25	7.22	147	176	255	174	313	116	93.9	10.3	37.7	226	74.5	19.9	0.712936	18	-9.44	0.06
20120618F	09:35	6.20	136	156	230	133	287	134	77.0	10.6	33.3	219	48.4	12.3	0.713138	32	-10.24	0.03
20120726F	09:10	6.30	218	245	202	40	423	241	73.5	9.9	43.2	188	22.7	7.3	0.714105	12	-10.12	0.13
20120728F	09:05	5.82	257	292	238	43	529	135	96.1	11.4	52.5	258	45.1	13.7	0.713875	42	-10.08	0.10
20120730F	09:30	6.70	216	248	206	38	438	201	93.1	10.1	44.6	188	32.7	9.1	0.713947	11	-10.96	0.12
20120801F	08:35	7.15	298	344	282	47	640	223	134	31.3	63.0	302	31.9	8.0	0.713795	28	n.d.	n.d.
20120802F	19:35	6.85	280	318	247	44	584	269	112	14.1	57.9	232	34.5	8.8	0.714027	14	n.d.	n.d.
20120803F	08:55	6.87	283	323	253	46	602	265	113	12.6	59.1	211	41.8	9.1	0.713969	4	n.d.	n.d.
Supra-glacial sample																		
20120801SG	13:50	5.80	10	9	16	14	9	n.d.	3.0	2.1	2.4	51.1	2.8	0.4	0.719761	37	n.d.	n.d.
Snow (S) and rain (R) samples																		
20120527S	n.d.	n.d.	1	2	20	12	8	n.d.	0.2	0.1	0.7	36.2	0.0	0.0	0.710028	1	n.d.	n.d.
20120614S	n.d.	n.d.	1	0	14	14	8	n.d.	1.1	0.2	0.8	73.9	4.6	1.5	0.711270	40	n.d.	n.d.
20120803R	n.d.	n.d.	32	6	53	75	15	n.d.	2.5	13.9	2.7	237	31.5	9.0	0.710681	10	n.d.	n.d.

[1]n=3

n.d. = not determined

Table S-3 Major element, trace element and Sr and Nd radiogenic isotopic compositions of leachate and residue samples. The bulk rock compositions are from Hindshaw *et al.*, 2018. 'R' samples are rock samples: R3 is a sandstone and R1, R2 and R4 are shales. 'S' samples are unconsolidated sediment samples: S1 is a glacial sediment sample.

Sample	Al	Fe	Ti	Mg	Ca	Na*	K	P	Mn	Ba	Sr	Rb	Nd	Sm	$^{87}Sr/^{86}Sr$	2SD[1]	εNd	2SD[2]
	mg/kg	mg/kg	mg/kg	mg/kg	mg/kg	mg/kg	mg/kg	mg/kg	mg/kg	mg/kg	mg/kg	mg/kg	mg/kg	mg/kg		(ppm)		
Acetic Acid (AA) Leach																		
R1-AA	83	46	b.d.l.	629	1159	n.m.	467	2.4	32.6	60.4	12.1	0.28	4.05	1.10	0.713461	40	-8.7	1.1
R2-AA	41	23	b.d.l.	723	1205	n.m.	285	2.3	73.5	45.3	18.1	0.12	2.15	0.65	0.713308	15	-8.3	0.4
R3-AA	66	766	b.d.l.	455	22628	n.m.	248	2.1	139	42.2	74.9	0.14	1.52	0.32	0.722740	3	-22.1	0.5
R4-AA	94	42	b.d.l.	536	702	n.m.	481	0.7	4.5	10.7	11.2	0.39	0.16	0.05	0.728661	20	-12.9	0.1
S1-AA	55	290	b.d.l.	644	2016	n.m.	204	1.3	146	38.7	8.0	0.12	0.48	0.14	0.725235	29	-15.8	1.0
0.005M Hydroxylamine Hydrochloride Leach																		
R1-HH	19	21	b.d.l.	26	b.d.l.	n.m.	60	54.2	9.6	2.9	0.8	0.05	0.05	0.02	0.710722	6	-8.4	1.1
R2-HH	11	6	b.d.l.	28	b.d.l.	n.m.	36	63.8	11.5	2.3	0.6	0.02	0.04	0.02	0.711622	4	-8.7	1.3
R3-HH	97	1707	b.d.l.	590	17106	n.m.	27	3.1	114	17.5	47.5	0.05	1.12	0.22	0.721645	22	-22.0	0.1
R4-HH	12	16	b.d.l.	15	35	n.m.	41	98.9	0.4	0.8	0.5	0.06	0.01	0.00	0.724296	12	n.m.	0.6
S1-HH	11	120	b.d.l.	78	117	n.m.	16	13.7	15.1	5.2	1.0	0.02	0.08	0.03	0.726981	48	-16.0	0.1
	Al_2O_3	Fe_2O_3	TiO_2	MgO	CaO	Na_2O	K_2O	P	Mn	Ba	Sr	Rb	Nd	Sm	$^{87}Sr/^{86}Sr$	2SD[1]	εNd	2SD[2]
	wt%	wt%	wt%	wt%	wt%	wt%	wt%	mg/kg	mg/kg	mg/kg	mg/kg	mg/kg	mg/kg	mg/kg		(ppm)		
Residue / detrital fraction																		
R1-d	16.1	8.8	1.0	1.4	b.d.l.	1.2	2.6	994	376	374	91	105	29.4	4.9	0.726781	32	-12.7	1.4
R2-d	22.0	12.4	1.0	1.9	b.d.l.	0.5	3.4	1372	435	465	101	150	33.9	5.9	0.729306	49	-11.4	1.0
R3-d	14.2	6.0	0.8	1.3	b.d.l.	1.4	2.7	514	306	509	75	101	29.4	4.7	0.756537	33	-24.1	1.0
R4-d	25.8	5.2	1.2	1.7	b.d.l.	0.8	4.8	353	181	733	153	221	46.1	7.8	0.744500	16	-18.6	0.2
S1-d	26.0	8.7	1.1	1.8	b.d.l.	1.0	5.2	594	466	953	136	218	41.7	6.8	0.757131	14	-23.0	0.5
*Bulk***																		
R1 (R01)	15.7	7.1	0.8	1.4	0.4	1.1	2.4	928	497	438	98	103	32.4	6.0	0.724490	17	-11.9	0.0
R2 (G)	16.0	7.7	0.8	1.4	0.3	1.1	2.4	1037	613	425	100	103	32.3	6.0	0.725796	28	-12.1	1.0
R3 (R03)	8.6	3.3	0.6	0.9	6.1	1.1	1.5	465	480	366	139	54	25.4	4.5	0.732295	14	-24.2	0.2
R4 (R04)	18.5	3.5	0.9	1.3	0.2	0.7	3.2	374	190	542	107	147	39.3	6.6	0.743564	32	-19.8	0.7
S1 (D)	18.3	6.7	0.8	1.5	0.5	0.9	3.3	479	735	706	99	135	36.5	6.5	0.752425	36	-23.3	0.2

b.d.l. = below detection limit, n.m. = not measured

*Na concentrations for the leachates are not reported as the leaching solution contained Na.

**The sample names in brackets were used in Hindshaw *et al.* (2018).

[1]n=3, [2]n=2

Table S-4 Fraction of Sr, Ca and Nd in the leachate samples. Concentrations in the leachate and bulk samples are reported in Table S-3. The Ca content in R1 and R2 HH leachates is 0 because the Ca concentrations were below the detection limit.

Sample	Strontium		Calcium		Neodymium	
	f-AA	f-HH	f-AA	f-HH	f-AA	f-HH
R1	0.12	0.01	0.45	0	0.12	0.00
R2	0.18	0.01	0.50	0	0.07	0.00
R3	0.54	0.34	0.52	0.39	0.06	0.04
R4	0.10	0.00	0.58	0.03	0.00	0.00
S1	0.08	0.01	0.54	0.03	0.01	0.00

Table S-5 Rare earth element (REE) concentrations of the leachate, residual and bulk samples. Bulk data is taken from Hindshaw *et al.*, 2018. REE patterns relative to UCC and PAAS are depicted in Fig. S-4.

Sample	La	Ce	Pr	Nd	Sm	Eu	Gd	Tb	Dy	Ho	Er	Tm	Yb	Lu
Acetic Acid (AA) Leach ($\mu g\ kg^{-1}$)														
R1-AA	1523	3773	729	4046	1104	265	1293	155	717	119	257	28.1	136	19.0
R2-AA	748	1827	355	2150	647	163	802	98.8	478	81.5	178	19.4	99.0	14.6
R3-AA	1548	3128	381	1520	324	86.3	346	56.6	325	62.6	164	22.1	124	17.2
R4-AA	117	288	36.7	156	45.1	12.0	71.1	10.2	51.1	8.9	22.4	3.1	18.0	2.6
S1-AA	322	806	101	479	136	35.1	179	24.6	127	23.0	56.9	7.2	40.2	5.8
0.005M Hydroxylamine Hydrochloride Leach ($\mu g\ kg^{-1}$)														
R1-HH	10.5	40.1	8.3	46.8	17.1	4.0	15.8	1.8	7.9	1.1	2.2	0.3	1.5	0.2
R2-HH	9.2	35.0	7.5	42.5	16.6	3.9	15.6	1.8	7.2	1.0	2.1	0.2	1.3	0.2
R3-HH	1388	2787	312	1122	221	55.1	217	35.3	196	36.4	92.0	12.0	66.0	8.3
R4-HH	3.1	10.3	1.8	10.4	4.8	1.2	6.3	0.6	2.2	0.3	0.6	0.1	0.3	0.0
S1-HH	23.8	83.2	14.3	76.9	29.1	7.1	32.6	3.7	15.1	2.1	4.1	0.5	2.5	0.3
*Residue / detrital fraction ($mg\ kg^{-1}$)**														
R1-d	37.4	70.6	8.1	29.4	4.9	1.0	3.6	0.6	3.4	0.7	2.0	0.3	2.0	0.3
R2-d	42.5	81.8	9.4	33.9	5.9	1.2	4.6	0.8	4.4	0.9	2.5	0.4	2.5	0.4
R3-d	38.5	74.7	8.2	29.4	4.7	0.8	2.8	0.4	2.0	0.4	1.0	0.1	0.8	0.1
R4-d	56.5	112.1	12.5	46.1	7.8	1.4	5.1	0.8	4.3	0.8	2.4	0.4	2.2	0.3
S1-d	53.4	104.1	11.5	41.7	6.8	1.2	4.2	0.7	3.6	0.7	1.8	0.3	1.7	0.2
*Bulk ($mg\ kg^{-1}$)**														
R1	35.7	71.2	8.4	32.4	6.0	1.2	4.5	0.7	4.0	0.7	2.0	0.3	1.9	0.3
R2	35.7	70.4	8.3	32.3	6.0	1.3	4.6	0.7	4.2	0.8	2.3	0.3	2.2	0.3
R3	30.5	60.3	6.8	25.4	4.5	0.9	3.1	0.4	2.2	0.4	1.0	0.1	0.9	0.1
R4	49.1	95.4	10.7	39.3	6.6	1.3	4.0	0.7	3.5	0.7	1.9	0.3	1.8	0.2
S1	43.9	88.5	9.9	36.5	6.5	1.2	4.3	0.6	3.3	0.6	1.6	0.2	1.4	0.2

*The hotplate digestion method used in this study does not digest zircons and therefore the high rare earth element (HREE) concentrations may be lower than the true total. Nd and Sm are fully digested by the hotplate method (Rickli *et al.*, 2013).

Supplementary Information References

Aciego, S.M., Bourdon, B., Lupker, M., Rickli, J. (2009) A new procedure for separating and measuring radiogenic isotopes (U, Th, Pa, Ra, Sr, Nd, Hf) in ice cores. *Chemical Geology* 266, 194-204.

Amiotte Suchet, P., Probst, J.L., Ludwig, W. (2003) Worldwide distribution of continental rock lithology: Implications for the atmospheric/soil CO2 uptake by continental weathering and alkalinity river transport to the oceans. *Global Biogeochemical Cycles* 17, 1038.

Arendt, C.A., Aciego, S.M., Sims, K.W.W., Robbins, M. (2015) Sequential separation of uranium, hafnium and neodymium from natural waters concentrated by iron coprecipitation. *Geostandards and Geoanalytical Research* 39, 293-303.

Aubert, D., Stille, P., Probst, A. (2001) REE fractionation during granite weathering and removal by waters and suspended loads: Sr and Nd isotopic evidence. *Geochimica et Cosmochimica Acta* 65, 387–406.

Bayon, G., Toucanne, S., Skonieczny, C., André, L., Bermell, S., Cheron, S., Dennielou, B., Etoubleau, J., Freslon, N., Gauchery, T., Germain, Y., Jorry, S.J., Ménot, G., Monin, L., Ponzevera, E., Rouget, M.-L., Tachikawa, K., Barrat, J.A. (2015) Rare earth elements and neodymium isotopes in world river sediments revisited. *Geochimica et Cosmochimica Acta* 170, 17-38.

Blaser, P., Lippold, J., Gutjahr, M., Frank, N., Link, J.M., Frank, M. (2016) Extracting foraminiferal seawater Nd isotope signatures from bulk deep sea sediment by chemical leaching. *Chemical Geology* 439, 189–204.

Cerling, T.E. (1984) The stable isotopic composition of modern soil carbonate and its relationship to climate. *Earth and Planetary Science Letters* 71, 229–240.

Channell, J.E.T., Hodell, D.A., Romero, O., Hillaire-Marcel, C., de Vernal, A., Stoner, J.S., Mazaud, A., Röhl, U. (2012) A 750-kyr detrital-layer stratigraphy for the North Atlantic (IODP Sites U1302-U1303, Orphan Knoll, Labrador Sea). *Earth and Planetary Science Letters* 317-318, 218–230.

Chapman, H., Bickle, M., Thaw, S.H., Thiam, H.N. (2015) Chemical fluxes from time series sampling of the Irrawaddy and Salween Rivers, Myanmar. *Chemical Geology* 401, 15-27.

Chen, T.-Y., Frank, M., Haley, B.A., Gutjahr, M., Spielhagen, R. F. (2012) Variations of North Atlantic inflow to the central Arctic Ocean over the last 14 million years inferred from hafnium and neodymium isotopes. *Earth and Planetary Science Letters* 353-354, 82-92.

Chester, R., Hughes, M.J. (1967) A chemical technique for the separation of ferro-manganese minerals, carbonate minerals and adsorbed trace elements from pelagic sediments. *Chemical Geology* 2, 249-262.

de Laeter, J.R., Böhlke, J.K., De Bièvre, P., Hidaka, H., Peiser, H.S., Rosman, K.J.R., Taylor, P.D.P. (2000) Atomic weights of the elements: review 2000. *Pure and Applied Chemistry* 75, 683-800.

Garçon, M., Chauvel, C., France-Lanord, C., Huyghe, P., Lavé, J. (2013) Continental sedimentary processes decouple Nd and Hf isotopes. *Geochimica et Cosmochimica Acta* 121, 177-195.

Garçon, M., Chauvel, C. (2014) Where is basalt in river sediments, and why does it matter? *Earth and Planetary Science Letters* 407, 61-69.

Goldberg, E.D., Koide, M., Schmitt, R.A., Smith, R.H. (1963) Rare-earth distributions in the marine environment. *Journal of Geophysical Research* 68, 4209–4217.

Gutjahr, M., Frank, M., Stirling, C.H., Klemm, V., van de Flierdt, T., Halliday, A.N. (2007) Reliable extraction of a deepwater trace metal isotope signal from Fe-Mn oxyhydroxide coatings of marine sediments. *Chemical Geology* 242, 35-370.

Haley, B.A., Klinkhammer, G.P., McManus, J. (2004) Rare earth elements in pore waters of marine sediments. *Geochimica et Cosmochimica Acta* 68, 1265–1279.

Haley, B.A., Frank, M., Spielhagen, R.F., Eisenhauer, A. (2008) Influence of brine formation on Arctic Ocean circulation over the past 15 million years. *Nature Geoscience* 1, 68-72.

Hannigan, R.E., Sholkovitz, E.R. (2001) The development of middle rare earth element enrichments in freshwaters: weathering of phosphate minerals. *Chemical Geology* 175, 495-508.

Helland-Hansen, W. (1990) Sedimentation in Paleogene Foreland Basin, Spitsbergen. *The American Association of Petroleum Geologists Bulletin* 74, 260-272.

Hindshaw, R.S., Lang, S.Q., Bernasconi, S.M., Heaton, T.H.E., Lindsay, M.R., Boyd, E.S. (2016a) Origin and temporal variability of unusually low δ13C-DOC values in two High Arctic catchments. *Journal of Geophysical Research: Biogeosciences* 121, 1073-1085.

Hindshaw, R.S., Heaton, T.H.E., Boyd, E.S., Lindsay, M.R., Tipper, E.T. (2016b) Influence of glaciation on mechanisms of mineral weathering in two high Arctic catchments. *Chemical Geology* 420, 37-50.

Hindshaw, R.S., Tosca, N.J., Piotrowski, A.M., Tipper, E.T. (2018) Clay mineralogy, strontium and neodymium isotope ratios in the sediments of two High Arctic catchments (Svalbard). *Earth Surface Dynamics* 6, 141-161.

Ilina, S.M., Viers, J., Lapitsky, S.A., Mialle, S., Mavromatis, V., Chmeleff, J., Brunet, P., Alekhin, Y.V., Isnard, H., Pokrovsky, O.S. (2013) Stable (Cu, Mg) and radiogenic (Sr, Nd) isotope fractionation in colloids of boreal organic-rich waters. *Chemical Geology* 342, 63-75.

Jacobsen, S.B., Wasserburg, G.J. (1980) Sm-Nd isotopic evolution of chondrites. *Earth and Planetary Science Letters* 50, 139-155.

Johannesson, K.H., Zhou, X. (1999) Origin of middle rare earth element enrichments in acid waters of a Canadian High Arctic lake. *Geochimica et Cosmochimica Acta* 63, 153–165.

Krogstad, E.J., Fedo, C.M., Eriksson, K.A. (2004) Provenance ages and alteration histories of shales from the Middle Archean Buhwa greenstone belt, Zimbabwe: Nd and Pb isotopic evidence. *Geochimica et Cosmochimica Acta* 68, 319-332.

Laukert, G., Frank, M., Bauch, D., Hathorne, E.C., Rabe, B., von Appen, W.-J., Wegner, C., Zieringer, M., Kassens, H. (2017) Ocean circulation and freshwater pathways in the Arctic Mediterranean based on a combined Nd isotope, REE and oxygen isotope section across Fram Strait. *Geochimica et Cosmochimica Acta* 202, 285-309.

Major, H., Haremo, P., Dallmann, W. K., Andresen, A. (2000) *Geological map of Svalbard 1:100 000*, sheet C9G Adventdalen, Temakart nr. 31, Norsk Polarinstitutt, Tromsø, Norway.

McLennan, S.M. (2001) Relationships between the trace element composition of sedimentary rocks and upper continental crust. *Geochemistry, Geophysics, Geosystems* 2, 2000GC000109.

Merschel, G., Bau, M., Schmidt, K., Münker, C., Dantas, E.L. (2017) Hafnium and neodymium isotopes and REY distribution in the truly dissolved, nanoparticulate/colloidal and suspended loads of rivers in the Amazon Basin, Brazil. *Geochimica et Cosmochimica Acta* 213, 383-399.

Mokadem, F., Parkinson, I.J., Hathorne, E.C., Anand, P., Allen, J.T., Burton, K.W. (2015) High-precision radiogenic strontium isotope measurements of the modern and glacial ocean: Limits on glacial-interglacial variations in continental weathering. *Earth and Planetary Science Letters* 415, 111-120.

Müller, R.D., Spielhagen, R.F. (1990) Evolution of the Central Tertiary Basin of Spitsbergen: towards a synthesis of sediment and plate tectonic history. *Palaeogeography Palaeoclimatology Palaeoecology* 80, 153-172.

Ohr, M., Halliday, A.N., Peacor, D.R. (1994) Mobility and fractionation of rare earth elements in argillaceous sediments: Implications for dating diagenesis and low-grade metamorphism. *Geochimica et Cosmochimica Acta* 58, 289–312.

Piotrowski, A.M., Banakar, V.K., Scrivner, A.E., Elderfield, H., Galy, A., Dennis, A. (2009) Indian Ocean circulation and productivity during the last glacial cycle. *Earth and Planetary Science Letters* 285, 179-189.

Pourmand, A., Dauphas, N., Ireland, T.J. (2012) A novel extraction chromatography and MC-ICP-MS technique for rapid analysis of REE, Sc and Y: Revising CI-chondrite and Post-Archean Australian Shale (PAAS) abundances. *Chemical Geology* 291, 38-54.

Rousseau, T.C.C., Sonke, J.E., Chmeleff, J., van Beek, P., Souhaut, M., Boaventura, G., Seyler, P., Jeandel, C. (2015) Rapid neodymium release to marine waters from lithogenic sediments in the Amazon estuary. *Nature Communications 6*, 7592.

Saltzman, M.R., Thomas, E. (2012) Carbon isotope stratigraphy. In: Gradstein, F., Ogg, J., Schmitz, M.D., Ogg, G. (Eds.) *The Geologic time scale*. Elsevier B.V., 207–232.

Schlegel, A., Lisker, F., Dörr, N., Jochmann, M., Schubert, K., Spiegel, C. (2013) Petrography and geochemistry of siliclastic rocks from the Central Tertiary Basin of Svalbard – implications for provenance, tectonic setting and climate. *Zeitschrift der Deutschen Gesellschaft für Geowissenschaften* 164, 173-186.

Shaw, H.F., Wasserburg, G.J. (1985) Sm-Nd in marine carbonates and phosphates: Implications for Nd isotopes in seawater and crustal ages. *Geochimica et Cosmochimica Acta* 49, 503–518.

Stevenson, E.I., Aciego, S.M., Chutcharavan, P., Parkinson, I.J., Burton, K.W., Blakowski, M.A., Arendt, C.A. (2016) Insights into combined radiogenic and stable strontium isotopes as tracers for weathering processes in subglacial environments. *Chemical Geology* 429, 33-43.

Tanaka, T., Togashi, S., Kamioka, H., Amakawa, H., Kagami, H., Hamamoto, T., Yuhara, M., Orihashi, Y., Yoneda, S., Shimizu, H., Kunimaru, T., Takahashi, K., Yanagi,

T., Nakano, T., Fujimaki, H., Shinjo, R., Asahara, Y., Tanimizu, M., Dragusanu, C. (2000) JNd-1: a neodymium isotopic reference in consistency with LaJolla neodymium. *Chemical Geology* 168, 279-281.

Tessier, A., Campbell, P.G.C., Bisson, M. (1979) Sequential extraction procedure for the speciation of particulate trace metals. *Analytical Chemistry* 51, 844–851.

Tricca, A., Stille, P., Steinmann, M., Kiefel, B., Samuel, J., Eikenberg, J. (1999) Rare earth elements and Sr and Nd isotopic compositions of dissolved and suspended loads from small river systems in the Vosges mountains (France), the river Rhine and groundwater. *Chemical Geology* 160, 139–158.

Viers, J., Wasserburg, G.J. (2004) Behavior of Sm and Nd in a lateritic soil profile. *Geochimica et Cosmochimica Acta* 68, 2043-2054.

Violette, A., Riotte, J., Braun, J.J., Oliva, P., Marechal, J.-C., Sekhar, M., Jeandel, C., Subramanian, S., Prunier, J., Barbiero, L., Dupré, B. (2010) Formation and preservation of pedogenic carbonates in South India, links with paleo-monsoon and pedological conditions: Clues from Sr isotopes, U-Th series and REEs. *Geochimica et Cosmochimica Acta* 74, 7059–7085.

Wilson, D.J., Piotrowski, A.M., Galy, A., Clegg, J.A. (2013) Reactivity of neodymium carriers in deep sea sediments: Implications for boundary exchange and paleoceanography. *Geochimica et Cosmochimica Acta* 109, 197-221.

Yde, J.C., Riger-Kusk, M., Christiansen, H.H., Knudsen, N.T., Humlum, O. (2008) Hydrochemical characteristics of bulk meltwater from an entire ablation season, Longyearbreen, Svalbard. *Journal of Glaciology* 54, 259-272.

Zamanian, K., Pustovoytov, K., Kuzyakov, Y. (2016) Pedogenic carbonates: Forms and formation processes. *Earth Science Reviews* 157, 1–17.